Int. J. Radiation Oncology Biol. Phys., Vol. ■, No. ■, pp. 1–9, 2010

0360-3016/$–see front matter

ELSEVIER

doi:10.1016/j.ijrobp.2010.02.020

**PHYSICS CONTRIBUTION**

# MELANIN-COVERED NANOPARTICLES FOR PROTECTION OF BONE MARROW DURING RADIATION THERAPY OF CANCER

Andrew D. Schweitzer, M.D.,*†‡ Ekaterina Revskaya, Ph.D.,* Peter Chu, B.Sc.,* Valeria Pazo, M.D.,§ Matthew Friedman,* Joshua D. Nosanchuk, M.D.,‖¶ Sean Cahill, Ph.D.,# Susana Frases, Ph.D.,¶ Arturo Casadevall, M.D., Ph.D.,‖¶ and Ekaterina Dadachova, Ph.D.*¶

Departments of *Nuclear Medicine, ‖Medicine, ¶Microbiology and Immunology, and #Biochemistry, Albert Einstein College of Medicine, Bronx, NY; †Howard Hughes Medical Institute–Medical Fellows Program, Chevy Chase, MD; ‡The Mount Sinai School of Medicine, New York, NY; and §Jacobi Medical Center, Bronx, NY

**Purpose: Protection of bone marrow against radiotoxicity during radioimmunotherapy and in some cases external beam radiation therapy such as hemi-body irradiation would permit administration of significantly higher doses to tumors, resulting in increased efficacy and safety of treatment. Melanin, a naturally occurring pigment, possesses radioprotective properties. We hypothesized that melanin, which is insoluble, could be delivered to the bone marrow by intravenously administrated melanin-covered nanoparticles (MNs) because of the human body's "self-sieving" ability, protecting it against ionizing radiation.**

**Methods and Materials: The synthesis of MNs was performed via enzymatic polymerization of 3,4-dihydroxyphenylalanine and/or 5-S-cysteinyl-3,4-dihydroxyphenylalanine on the surface of 20-nm plain silica nanoparticles. The biodistribution of radiolabeled MNs in mice was done at 3 and 24 h. Healthy CD-1 mice (Charles River Laboratories International, Inc., Wilmington, MA) or melanoma tumor–bearing nude mice were given MNs intravenously, 50 mg/kg of body weight, 3 h before either whole-body exposure to 125 cGy or treatment with 1 mCi of $^{188}$Re-labeled 6D2 melanin-binding antibody.**

**Results: Polymerization of melanin precursors on the surface of silica nanoparticles resulted in formation of a 15-nm-thick melanin layer as confirmed by light scattering, transmission electron microscopy, and immunofluorescence. The biodistribution after intravenous administration showed than MN uptake in bone marrow was 0.3% and 0.2% of injected dose per gram at 3 and 24 h, respectively, whereas pre-injection with pluronic acid increased the uptake to 6% and 3% of injected dose per gram, respectively. Systemic MN administration reduced hematologic toxicity in mice treated with external radiation or radioimmunotherapy, whereas no tumor protection by MNs was observed.**

**Conclusions: MNs or similar structures provide a novel approach to protection of bone marrow from ionizing radiation based on prevention of free radical formation by melanin.** 

**Melanin, Nanoparticles, Bone marrow, Radiation protection, Radioimmunotherapy.**

## INTRODUCTION

Bone marrow toxicity is the dose-limiting factor for both external beam radiation therapy (EBRT) and radioimmunotherapy (RIT) in cancer patients, such that doses over 200 cGy cause significant acute and long-term toxicity. For example, the $^{131}$I-labeled anti-CD20 monoclonal antibody (Bexxar; GlaxoSmithKline, Research Triangle Park, NC) is very effective in some patients with relapsed or refractory non-Hodgkin lymphoma, but doses in excess of 75 cGy are associated with severe hematologic toxicity in patients with low bone marrow reserves. Protection of bone marrow against harmful effects of radiation in such patients would permit administration of significantly higher doses of EBRT or RIT, which could translate into increased efficacy and safety of treatment.

Reprint requests to: Ekaterina Dadachova, Ph.D., Department of Nuclear Medicine, Albert Einstein College of Medicine, 1695A Eastchester Rd., Bronx, NY 10461. Tel: (718) 405-8485; Fax: (718) 405-8457; E-mail: edadacho@aecom.yu.edu

A. D. Schweitzer, E. Revskaya, and P. Chu contributed equally to this study.

A. D. Schweitzer was a Howard Hughes Medical Institute Medical Research Training Fellow. A. Casadevall and J. D. Nosanchuk were supported by National Institutes of Health award AI052733. The instrumentation in the Albert Einstein College of Medicine Structural NMR (Nuclear Magnetic Resonance) Resource is supported by the Albert Einstein College of Medicine and in part by grants from the National Science Foundation (DBI9601607 and DBI0331934), the National Institutes of Health (RR017998), and the Howard Hughes Medical Institute Research Resources for Biomedical Sciences.

Conflict of interest: none.

Received Sept 28, 2009, and in revised form Dec 15, 2009. Accepted for publication Feb 12, 2010.

Melanin pigments are ubiquitous in nature polymers with a variety of biological functions (1). Many fungi constitutively synthesize melanin (2), which is likely to confer a survival advantage in the environment by protecting against environmental predators, heavy metal toxicity, and physical insults such as ultraviolet and solar radiation (3). Melanized microorganisms inhabit some remarkably extreme environments on the planet including high-altitude, Arctic, and Antarctic regions (4). Melanized fungal species colonize the walls of the damaged reactor at Chernobyl and cooling pool water in nuclear reactors (5, 6). These findings and the laboratory observations of the resistance of melanized fungi to ionizing radiation (7, 8) suggest a role for this pigment in radioprotection. Recently, we showed that nonlethal doses of ionizing radiation (500 times above the background) change the electronic properties of melanin and enhance the growth of melanized fungi (9). Later, we investigated the radioprotective properties of fungal melanin by subjecting the melanized fungi to lethal doses of radiation (up to 8 kGy) and showed that chemical composition and spatial arrangement into spheres contributed toward the radioprotective properties of melanin (10). Until recently, the actual mechanism of radioprotection by melanin was unknown, and it was assumed to be a result of free radical scavenging of the highly destructive radicals generated by the radiolysis of water (11). Most recently, we have established that given melanin's numerous aromatic oligomers containing multiple $\pi$-electron systems (Fig. 1), a generated Compton recoil electron gradually loses energy while passing through the pigment, until its energy is sufficiently low that it can be trapped by stable free radicals present in the pigment. Controlled dissipation of high-energy recoil electrons by melanin prevents secondary ionizations and the generation of damaging free radical species (12). Because melanin is a natural product, these observations have encouraged the view that this pigment may find applications in radioprotection of humans.

One challenge in developing melanin for radioprotection is to direct the pigment to the bone marrow. The difficulty with conventional administration approaches is that melanin is not soluble in aqueous solvents, and free melanin is a variable mixture of micron-sized particles (13). Consequently, if melanin suspensions are given intravenously, significant numbers of particles will likely lodge in the lungs instead of bone marrow as a result of the human body's ability to ''self-sieve'' circulating particles according to their size. On the other hand, submicron particles of 20 to 100 nm tend to lodge in the bone marrow, and this phenomenon has been exploited in nuclear medicine practice, where bone marrow is routinely imaged by injecting a $^{99m}$Tc-labeled sulfur ''nanocolloid'' (14). Hence we hypothesized that nanoparticles can be used as carriers of melanin for delivery into the bone marrow, where they would protect hematopoietic cells against radiation fluxes during radiation therapy. We report the results of proof-of-principle experiments that establish the potential of melanin-covered nanoparticles (MNs) for protection against harmful effects of EBRT and RIT.

## METHODS AND MATERIALS

### *Kinetic measurements and $^1$H nuclear magnetic resonance of melanin intermediates*

To establish the time necessary for depositing several layers of melanin on the surface of nanoparticles, we performed kinetic experiments for polymerization of phenolic precursors into melanin. The kinetics was measured by spectrophotometry (measuring the absorbance of the solutions at a certain wavelength) of the reaction mixtures. The reaction conditions used for spectrophotometry measurements of 3,4-dihydroxyphenylalanine (L-DOPA) melanin formation were adapted from previously published sources (12, 15). Approximately 21 U of mushroom tyrosinase from Sigma (St. Louis, MO) (4 $\mu$g of 5,370 U/mg) was added to a 100-$\mu$L solution of 4.94-mg/mL L-DOPA in 0.05-mol/L sodium phosphate buffer, pH 6.8. By use of a SpectraMax 250 microplate reader (Molecular Devices, Sunnyvale, CA), spectrophotometry data were collected at 37°C over the range of 250 to 750 nm for up 180 minutes after start of the reaction.

To unambiguously identify the reaction intermediates leading to formation of melanin during enzymatic polymerization of L-DOPA, we performed $^1$H nuclear magnetic resonance (NMR) of the samples on a Bruker DRX 300-MHz spectrometer (Bruker Corp., Billerica, MA). The reaction solution consisted of 1.5 mg of L-DOPA in 0.6 mL of 0.05-mol/L sodium phosphate buffer, pH 6.8, in deuterated water. The solution was then added to an NMR tube followed by 126 U of tyrosinase. The temperature was set to 37°C, and 1D proton spectra were collected in a 5-minute period by use of 96 interval scans, a sweep width of 20 ppm sampled with 16 k points, and a recycle delay of 2.8 seconds. Spectra were processed with a 0.5-Hz exponential window function.

### *High-performance liquid chromatography and mass spectrometry of melanin intermediates*

To confirm the results of $^1$H NMR on the identity of melanin intermediates, we analyzed products present in the reaction mixture by high-performance liquid chromatography, followed by mass spectrometry of each peak corresponding to a respective product. The chromatographic analysis of the composition of the reaction mixtures for presence of melanin intermediates was performed at 0, 5, and 20 minutes after the start of the reaction with a Time 0 sample taken for analysis before addition of tyrosinase. High-performance liquid chromatography was performed on an Alltima HP C18 aqueous reverse phase column (Alltech Associates, Inc, Deerfield, IL) with an internal diameter of 4.6 mm and a length of 250 mm. The mobile phase was 0.1% trifluoroacetic acid in water (solvent A) and 0.1% trifluoroacetic acid in acetonitrile (solvent B) at 1.0 mL/min with the elution gradient described previously (15, 16). Before the injection of tyrosinase-containing samples, tyrosinase was filtered out on a Millipore Microcon YM-10 Centrifugal Concentrator (Millipore, Billerica, MA) with a nominal molecular weight cutoff of 10,000 to prevent its interference with the column performance. The 14-minute fraction was collected and analyzed on an LTQ linear ion trap mass spectrometer (Thermo Fisher Scientific, Waltham, MA). Flow injection analysis was set at a flow rate of 50 $\mu$L/min of 50% acetonitrile/water containing 0.1% formic acid and was used to introduce the samples into the LTQ.

### *Preparation of MNs, size determination, and immunofluorescence with melanin-binding antibody*

Plain silica nanoparticles (20 nm in diameter) were purchased from Corpuscular, Inc. (Cold Spring, NY). On the basis of the

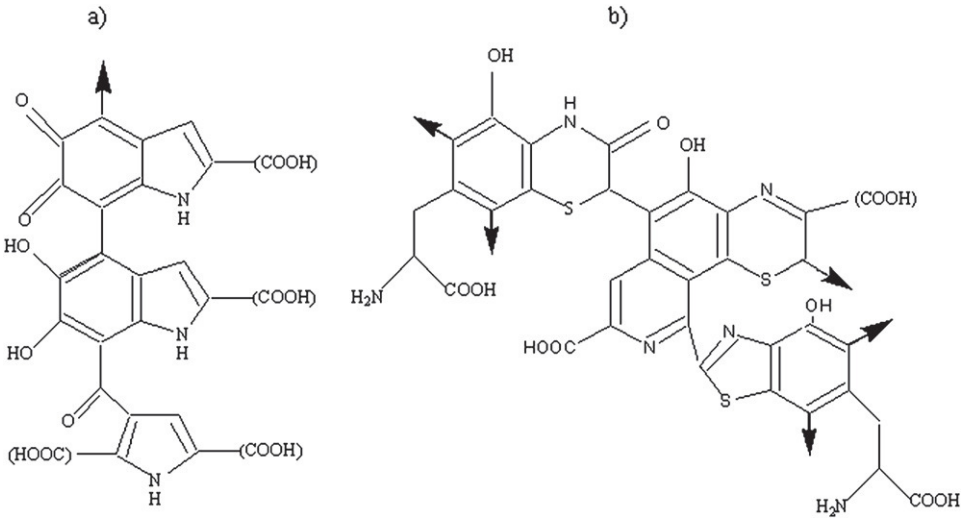


Fig. 1. Chemical structure of melanin: (a) structure of eumelanin oligomer and (b) structure of pheomelanin oligomer.

results of the kinetic experiments, overnight incubation was chosen as sufficient time for melanin formation on the nanoparticles surface. We incubated 1 mL of silica nanoparticle suspension (400-mg/mL solution) with constant agitation overnight at 37°C with melanin precursors and 215 U of mushroom tyrosinase (Sigma) in 800 $\mu$L of 0.2-mol/L phosphate buffer, pH 6.8, diluted with 600 $\mu$L of deionized water. The precursor for L-3,4-dihydroxyphenylalanine (L-DOPA) melanin was 10 mg of L-DOPA, whereas L-DOPA/5-S-cysteinyl-3,4-dihydroxyphenylalanine (5-S-cysteinyl-DOPA) melanin was generated from a mixture of 15.76 mg of 5-S-cysteinyl-DOPA and 0.4 mg of L-DOPA. After incubation, 20 $\mu$L of 6-mol/L hydrochloric acid was added to the reaction mixture to halt the reaction by lowering the pH level to approximately 3. The MNs were dialyzed extensively against deionized water and then phosphate-buffered saline solution. Effective diameters of MNs were determined by dynamic light scattering on a Zeta Potential analyzer (Brookhaven Instruments, Holtsville, NY). The MN suspensions were diluted 30-fold and sonicated for 5 minutes before Zeta Potential analysis. The MNs were imaged by transmission electron microscopy at the Analytical Imaging Facility, Albert Einstein College of Medicine. To confirm that the material deposited on the spheres was melanin, the MNs were incubated with the melanin-binding antibody 6D2 and imaged by indirect immunofluorescence as described previously (17).

### *Radiolabeling of MNs with $^{188}$Re and biodistribution in CD-1 mice*

To test the hypothesis that MNs will lodge themselves in the bone marrow after intravenous (IV) administration, we quantified the uptake of MNs in the bone marrow and other organs by radiolabeling them with $^{188}$Re. For animal experiments described in this article, all procedures followed the guidelines of the Institute for Animal Studies, Albert Einstein College of Medicine. Melanin-covered nanoparticles were combined with 0.4 mL of $Na^{188}ReO_4$ in normal saline solution, 20 mg of sodium gluconate, and 20 $\mu$L of 20-mg/mL $SnCl_2$ and incubated at 37°C for 1 h. The $^{188}$Re MNs were separated from the supernatant and diluted with phosphate-buffered saline solution. To ascertain the stability of $^{188}$Re attachment to the MNs, they were incubated with mouse serum at 37°C for 24 h, and at 1, 3, 6 and 24 h, they were analyzed by silica gel instant thin layer chromatography by use of strips presoaked in 10% bovine serum albumin. For the biodistribution experiment, $^{188}$Re MNs were injected intravenously into groups of five CD-1 mice (Charles River Laboratories International, Inc., Wilmington, MA) at 50 mg/kg of body weight. The uptake of $^{188}$Re MNs in bone marrow and major organs was measured with and without pre-administration of pluronic acid, 30 mg/kg of body weight, which minimizes interaction of nanoparticles with the reticuloendothelial cells in the liver and spleen and redirects them into the bone marrow (18), given 12 h before the administration of radiation.

### *Protection of bone marrow from external and internal radiation with MNs*

In the first series of experiments, we injected CD-1 mice with 50-mg/kg MNs made with L-DOPA or with non-melanized nanoparticles (no pluronic acid was used in these experiments) and irradiated mice 3 h later with 125 cGy of external gamma radiation from a $^{137}$Cs source delivered at a dose rate of 14 Gy/min. Mice were immobilized in the Styrofoam holder. Because irradiation lasted only 5.4 seconds, no anesthesia was used. The white blood cell (WBC) and platelet counts were monitored for 30 days. For platelet counts, the blood was collected from the tail vein into 200 $\mu$L of 1% ammonium oxalate, and platelets were counted manually in a hemocytometer, by use of phase contrast, at 400× magnification, as described previously (19). For WBC counts, blood was also collected from the tail vein and mixed with 0.5 mL of 2% acetic acid (vol/vol). After 30 seconds, 10 $\mu$L of the suspension was drawn into the hemocytometer chamber. Cells were allowed to settle for about 5 minutes and counted in ''four corners'' of the grid. For the calculations for the total number of cells per cubic millimeter, the following equation was used: Total WBC/mm$^3$ = [$N$/(4 mm$^2$) (0.1 mm)] × 20, where $N$ is the number of WBCs counted on each side of the hemocytometer grid (19).

In the second series of experiments, we used A2058 human metastatic melanoma tumors in nude mice (Charles River Laboratories International, Inc.) to evaluate the ability of MNs to protect bone marrow during RIT. We have used this animal model for the development of radionuclide therapy of metastatic melanoma (20, 21). Female mice aged 6 to 8 weeks were injected subcutaneously with 8 × 10$^6$ A2058 cells into the right flank. When tumors in mice reached 3 to 5 mm in diameter, they were randomized into groups of five. Group 1 was given 50-mg/kg MNs made with

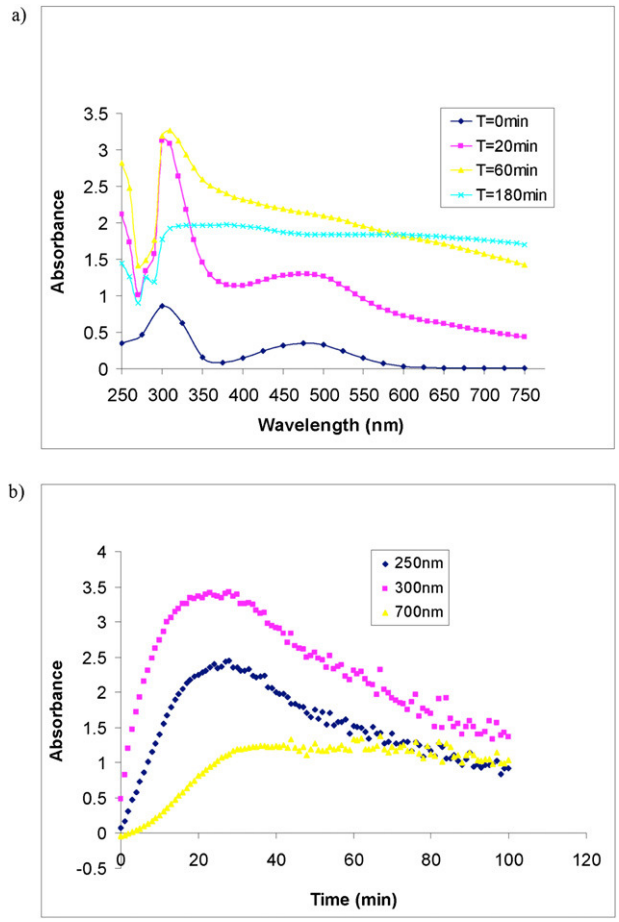


Fig. 2. Spectrophotometry evaluation of melanin formation from 3,4-dihydroxyphenylalanine (catalyzed by tyrosinase): (a) absorption of reaction mixtures in 250- to 750-nm range at 0 to 180 minutes after the start of the reaction and (b) kinetics of melanin formation over the period of 100 minutes was followed at 250, 300, and 700 nm.

L-DOPA/5-S-cysteinyl-DOPA 3 h before being treated with RIT (1 mCi of $^{188}$Re-labeled melanin-binding monoclonal antibody 6D2), whereas Group 2 received only RIT treatment. Group 3 was left untreated. Tumor volumes were measured immediately before administration of RIT and every 3 to 4 days thereafter for 30 days by measuring three dimensions with calipers, and the volume was calculated by multiplying the product of the three perpendicular measurements by 0.5, assuming an elliptical geometry.

### *Statistical analysis*

The Student *t* test for unpaired data was used to analyze differences in the organ uptake in the biodistribution studies, WBC and platelet counts, and tumor size in radioprotection studies (Prism software; GraphPad, San Diego, CA). The sample sizes in animal experiments were pre-planned. Differences were considered statistically significant at $P < 0.05$.

## RESULTS

### *Kinetics of melanin synthesis*

Spectrophotometry evaluation in the range of 250 to 750 nm of L-DOPA/tyrosinase reaction products formed at 0 to 180 minutes from the start of the reaction showed a major absorbance peak at 300 nm (Fig. 2a). Therefore the kinetics of melanin formation over the period of 100 minutes was followed at 250, 300, and 700 nm. For all three wavelengths, a sharp rise in absorption was observed after 10 to 25 minutes accompanied by development of yellowish-red coloration that progressed to black after 50 minutes, which was consistent with the presence of melanin (Fig. 2b).

Melanin synthesis proceeds through 5,6-dihydroxyindole (5,6-DHI) intermediate. High-performance liquid chromatography analysis of the reaction mixture at 0 minutes showed a single peak of L-DOPA at 9 minutes. At 5 minutes after the start of the reaction, additional peaks appeared, at 10 to 11 minutes, as well as several prominent peaks at 14 to 16 minutes (Fig. 3a). At 20 minutes after start of the reaction, the intensity of the peak at 14.5 minutes increased (Fig. 3b). The mass spectrometry analysis of the latter peak yielded 150.1 *m*/*z* for the molecular ion, implying the presence of 5,6-DHI (molecular weight, 149) intermediate. $^{1}$H NMR of the reaction mixture performed at 0 minutes showed L-DOPA signals at 6.7 to 7.0, 3.3, and 3 ppm and the residual water peak at 4.7 ppm (Fig. 4). The signals that appeared after 5 minutes and grew steadily with time were from 5,6-DHI (chemical shifts at 7.2–7.1 and 6.5 ppm). The peaks at 6.6

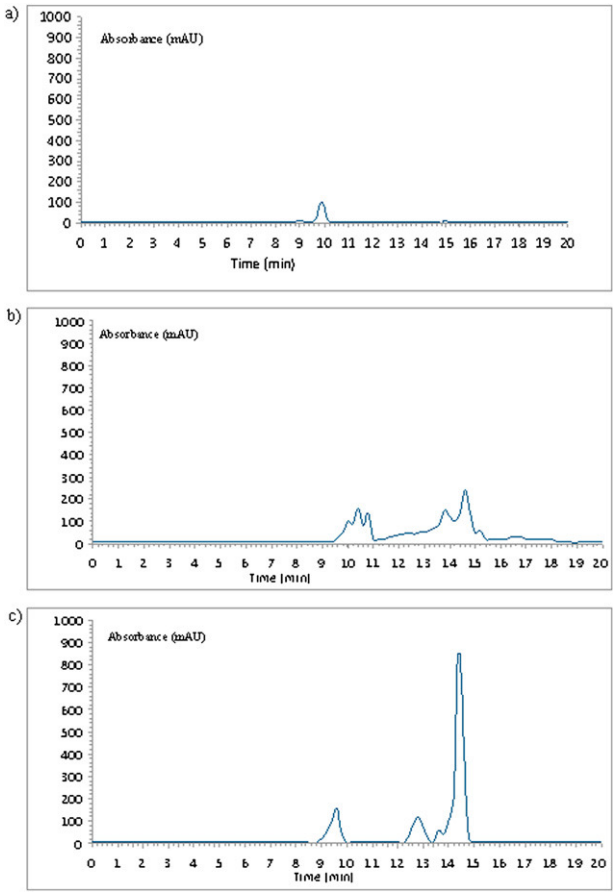


Fig. 3. High-performance liquid chromatography of 3,4-dihydroxyphenylalanine/tyrosinase reaction mixture during various stages of melanin synthesis: (a) 0 minutes (before addition of tyrosinase), (b) 5 minutes after start of reaction, and (c) 20 minutes after start of reaction.

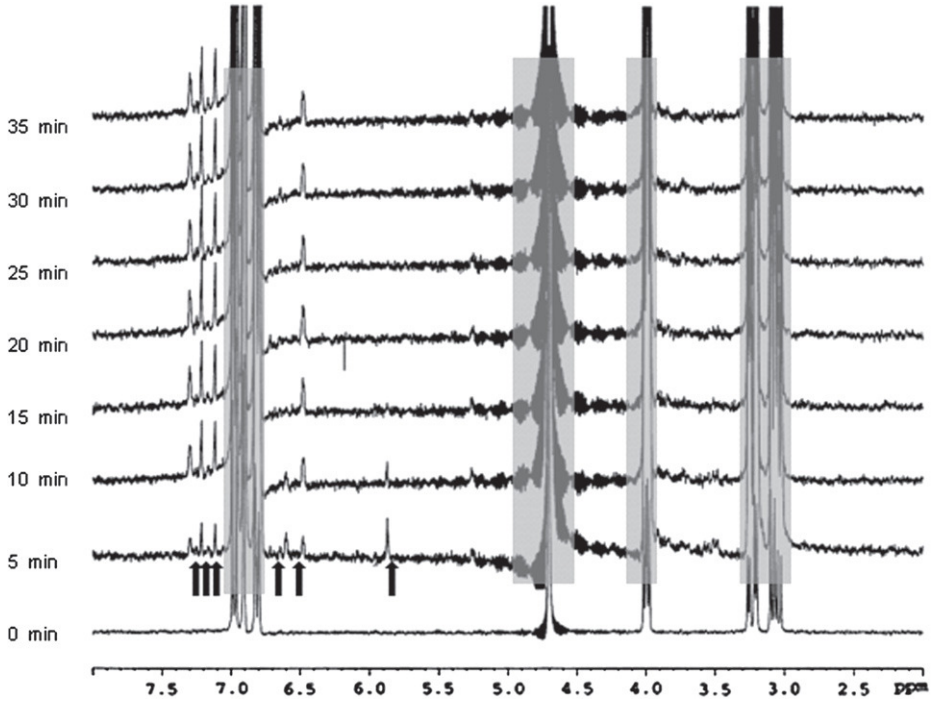


Fig. 4. $^{1}$H nuclear magnetic resonance of 3,4-dihydroxyphenylalanine (L-DOPA) solutions during various stages of melanin synthesis. The lowest spectrum represents L-DOPA solution before the addition of tyrosinase, and the spectra above are marked with the times passed after the addition of tyrosinase to L-DOPA. Arrows indicate melanin intermediate–associated peaks. Opaque gray regions represent background L-DOPA peaks and the residual water peak at 4.7 ppm.

and 5.9 ppm, which appeared at 5 minutes and disappeared after 10 minutes, could be assigned to leucodopachrome.

*Melanization of silica nanoparticles*

The overnight incubation of 20-nm silica nanoparticles with L-DOPA or L-DOPA/5-S-cysteinyl-DOPA in the presence of tyrosinase resulted in the formation of black or brown suspensions. To investigate the effective diameter of these MNs, 30-fold dilutions of sonicated plain nanoparticles or MNs were prepared for measurement in the light-scattering Zeta Potential analyzer. The diameter of plain nanoparticles determined by this technique proved to be 30.8 nm, that of MNs made with L-DOPA was 58.4 nm, and that of MNs made with L-DOPA/5-S-cysteinyl-DOPA was 61.7 nm (Figs. 5a–5c). These measurements were confirmed by transmission electron microscopy of MNs (Fig. 5d). Because the diameter of MNs approximately doubled in comparison with the initial plain nanoparticles, the thickness of the melanin layer on the surface of MNs was estimated to be $(60 - 30)/2 = 15$ nm. Finally, to confirm the identity of the pigment on the surface of MNs as melanin, immunofluorescence of the particles was performed with a melanin-binding monoclonal antibody 6D2 (17), and this monoclonal antibody was observed to bind avidly to the surface of MNs, thus confirming the presence of melanin (Fig. 5e).

*Biodistribution of MNs in mice*

To trace the behavior of MNs *in vivo*, they were radiolabeled with $^{188}$Re. The attachment of $^{188}$Re label to MNs was stable in mouse serum at 37°C for at least 24 h (data not shown). The results of the biodistribution study at 3 and 24 h after IV administration showed that when MNs by themselves were injected, the uptake in the bone marrow was 0.3% and 0.2% of injected dose per gram at 3 and 24 h, respectively (Fig. 6a). Pre-injection of mice with pluronic acid 12 h before administration of MNs elevated their uptake in the bone marrow to 6% and 3% of injected dose per gram at 3 and 24 h, respectively (Fig. 6b). Without pre-injection with pluronic acid, most of the MNs localized in the liver and spleen by 3 h, with the uptake in these two organs staying the same ($p > 0.05$) at 24 h (Fig. 6a). Pre-injection with pluronic acid elevated uptake in all organs at 3 h (Fig. 6b); however, by 24 h after injection, the uptake of MNs in all organs except for the bone marrow and lungs decreased dramatically in comparison with 3-h values ($p < 0.05$). No side effects associated with MN administration were seen in mice.

Melanin-covered nanoparticles protected mouse bone marrow during whole-body irradiation and RIT. In the first series of experiments, CD-1 mice received 50–mg/kg of body weight MNs made with L-DOPA or plain nanoparticles followed 3 h later by 125 cGy of external gamma radiation. Monitoring the WBC and platelet counts showed that for both cell types, there was no difference in cell counts in all groups on Day 3 ($p > 0.05$); on Day 5, there were higher numbers of WBCs in mice treated with MNs and non-melanized particles than in unprotected controls ($p = 0.02$); and for platelet counts on Day 5, there were higher counts in the MN group in comparison with the non-melanized particle group ($p = 0.01$) and with unprotected controls ($p = 0.04$). On Day 10 after irradiation, there were higher numbers of

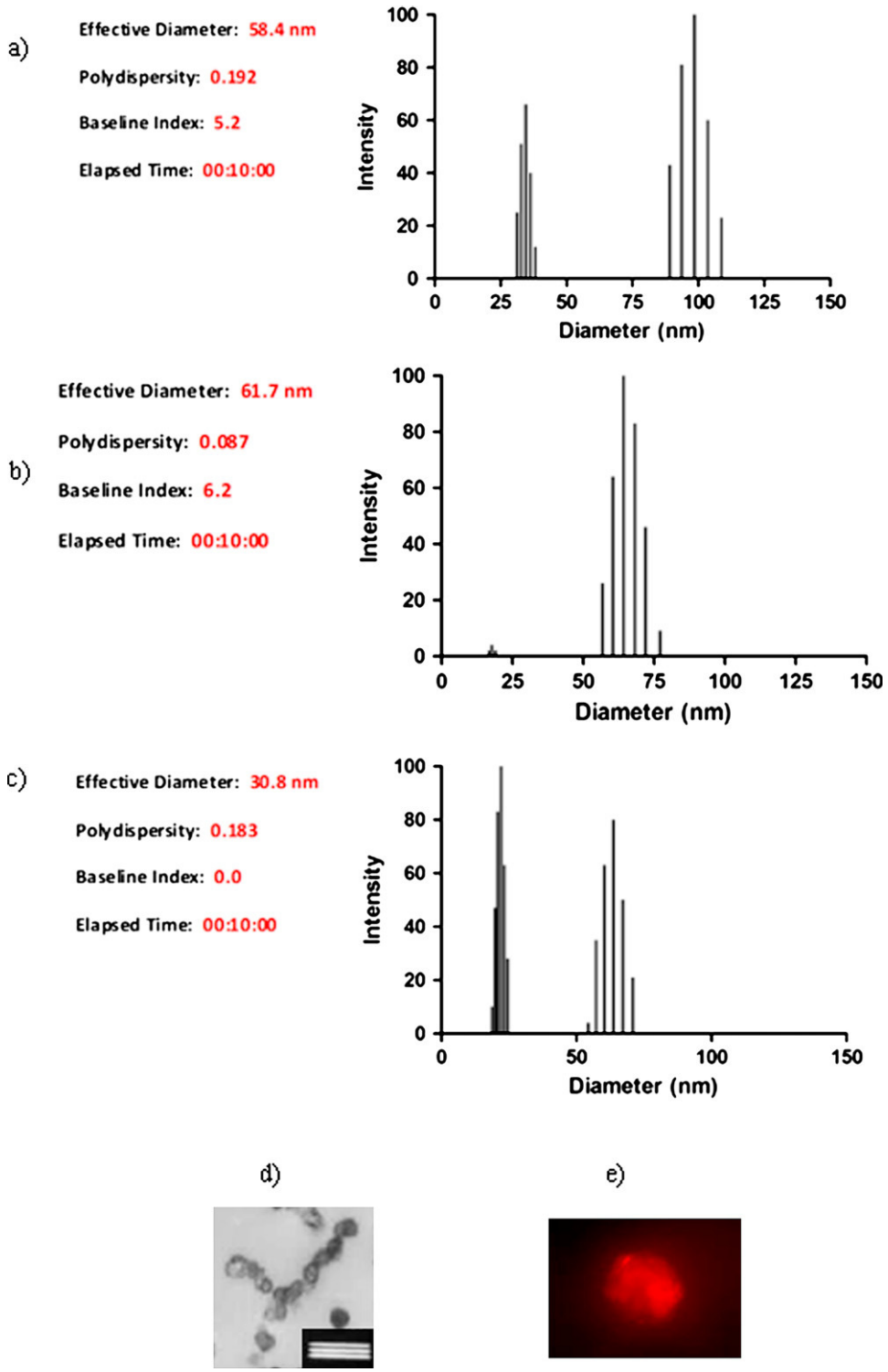


Fig. 5. Characterization of melanin-covered nanoparticles (MNs). (a–c) Particle size determination by light scattering: (a) MNs made with 3,4-dihydroxyphenylalanine (L-DOPA), (b) MNs made with L-DOPA/5-S-cysteinyl-DOPA, and (c) plain silica nanoparticles. (d) Transmission electron microscopy image of MNs made with L-DOPA. The bar is 200 nm. (e) Immunofluorescence image of MNs made with L-DOPA obtained with 6D2 melanin-binding antibody.

WBCs in the MN group in comparison with the non-melanized particle group ($p$ = 0.02) and with unprotected controls ($p$ = 0.004); in addition, there were significantly more platelets in the blood of MN-treated mice than in the non-melanized particle group or in unprotected controls ($p$ = 0.002) (Figs. 7a, 7b). In the second series of experiments, we used A2058 human metastatic melanoma tumors in nude mice to evaluate the ability of MNs to protect bone marrow during RIT. Given that nanoparticles in general are taken up to some degree by all tissues in the body because of their

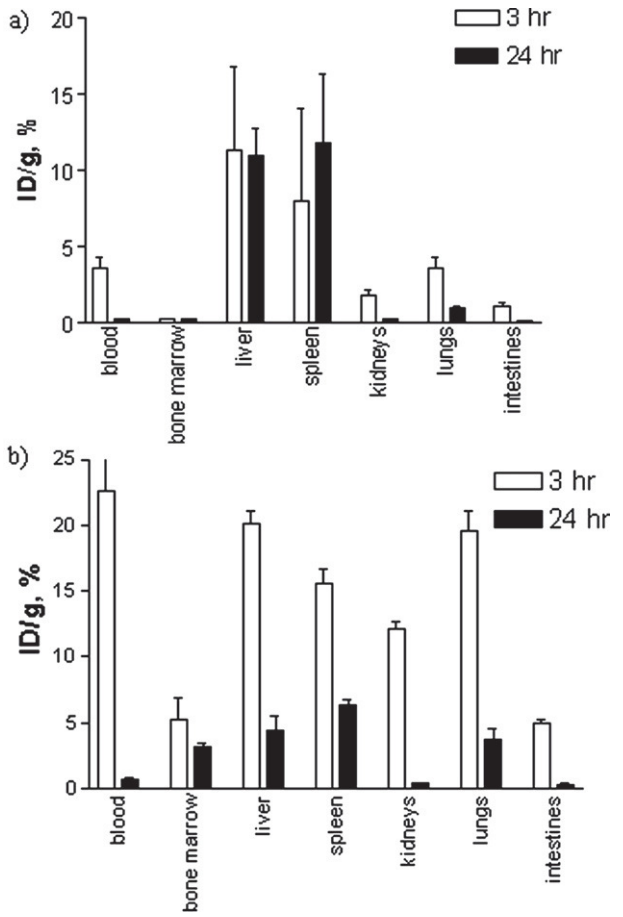


Fig. 6. Biodistribution of intravenously injected melanin-covered nanoparticles (MNs) made with 3,4-dihydroxyphenylalanine (L-DOPA) in CD-1 mice: (a) particles only and (b) pre-injection with pluronic acid 12 h in advance. There was an approximately 30-fold increase in the uptake of MNs in the bone marrow after pre-injection of pluronic acid. The error bars represent standard error of the mean. ID/g = injected dose per gram.

small size, we also investigated whether MN administration would protect the tumor from the cytocidal radiation, which would be an undesirable effect. Although tumors in untreated mice grew aggressively, there was significant retardation of tumor growth in RIT-treated mice both in combination with MNs and without MNs ($p < 0.01$), and no difference was observed between these two groups, indicating that MN administration did not interfere with the efficacy of RIT ($p = 0.06$) (Fig. 7c). In contrast, the drop in WBC counts between Days 3 and 7 after RIT treatment was significantly less in mice pretreated with MNs than in the RIT-only group ($p = 0.005$) (Fig. 7d), implying a protective effect of MNs against bone marrow toxicity due to RIT.

## DISCUSSION

Our results provide a proof-of-principle for the concept that directing the radioprotective melanin pigment into the bone marrow reduces the susceptibility of treated mice to the myelotoxic effects of therapeutic radiation. Hence melanin-coated nanospheres provide a novel approach for protection against radiation, and this approach may find uses in cancer therapy, preparedness against nuclear attacks, and prolonged space travel.

The availability of radioprotective agents that could be given before radiation exposure would alleviate some problems caused by exposure to ionizing radiation and might allow for significant increases in radiation dosing. However, after many years of research effort, only one potential approach has emerged so far: administration of free radical scavengers such aminothiols and phosphorothioates. Amifostine, also known as ethiofos, ethyol, or WR-2721 (MedImmune, Gaithersburg, MD), is a prodrug and must be metabolized to an active form (WR-1065) to be effective. It has been under evaluation in mice as a radioprotector (22) and for an adjunctive role in chemoradiation therapy of cervical cancer (23) and prostate cancer (24). Drawbacks of this drug are its relatively low radioprotective properties and potentially serious side effects, such as anaphylaxis. Melanin pigment delivered by MNs to the bone marrow offers a different approach to radioprotection by combination of controlled dissipation of high-energy recoil electrons that prevents the generation of free radical species and of free radical scavenging (12).

Kinetic experiments with tyrosinase-catalyzed melanin synthesis showed that melanin formation from L-DOPA in our system occurred within approximately 2 h via the classical pathway. In this reaction the sequence of compound generation is DOPA → dopaquinone → leucodopachrome → 5,6-DHI → eumelanin (25), with 5,6-DHI, the last intermediate before melanin formation, being prominently represented in the reaction mixture by 14 minutes after the start of the reaction, which was confirmed by mass spectrometry and $^{1}$H NMR. Thus overnight incubation with melanin precursors would be sufficient to allow for the deposition of multiple melanin layers on the surface of plain silica particles. Although the diameter of nanoparticles doubled after melanization, it still remained under 100 nm, a size appropriate for the delivery of nanoparticles into the bone marrow via the human body's ''self-sieving'' effect. The immunofluorescence with melanin-binding antibody confirmed the identity of the coating on the nanoparticles as melanin.

The radiolabeling of MNs with $^{188}$Re proved to be stable, probably because of the firm attachment of $[^{188}ReO]^{3+}$ species to multiple reactive sites on melanin (26). Pre-injection of mice with pluronic acid efficiently (more than 30-fold) redirected MNs into the bone marrow, thus providing the potential for enhanced delivery of significant amounts of nanoparticles to bone marrow. Previous studies showed that after IV administration of 20- to 60-nm nanoparticles, 0.5% to 1% of injected nanoparticles reach the bone marrow, whereas the majority of nanomaterial is sequestered by the mononuclear phagocytes of the liver and, to a lesser degree, of the spleen (27). However, it was suggested that nanoparticles can be efficiently redirected into the bone marrow in rats by pretreatment or coadministration of block copolymers of the poloxamer series, for example, poloxamer-407 (polyethylene glycol/polyethylene oxide) (18), which minimizes interaction of nanoparticles with the reticuloendothelial cells

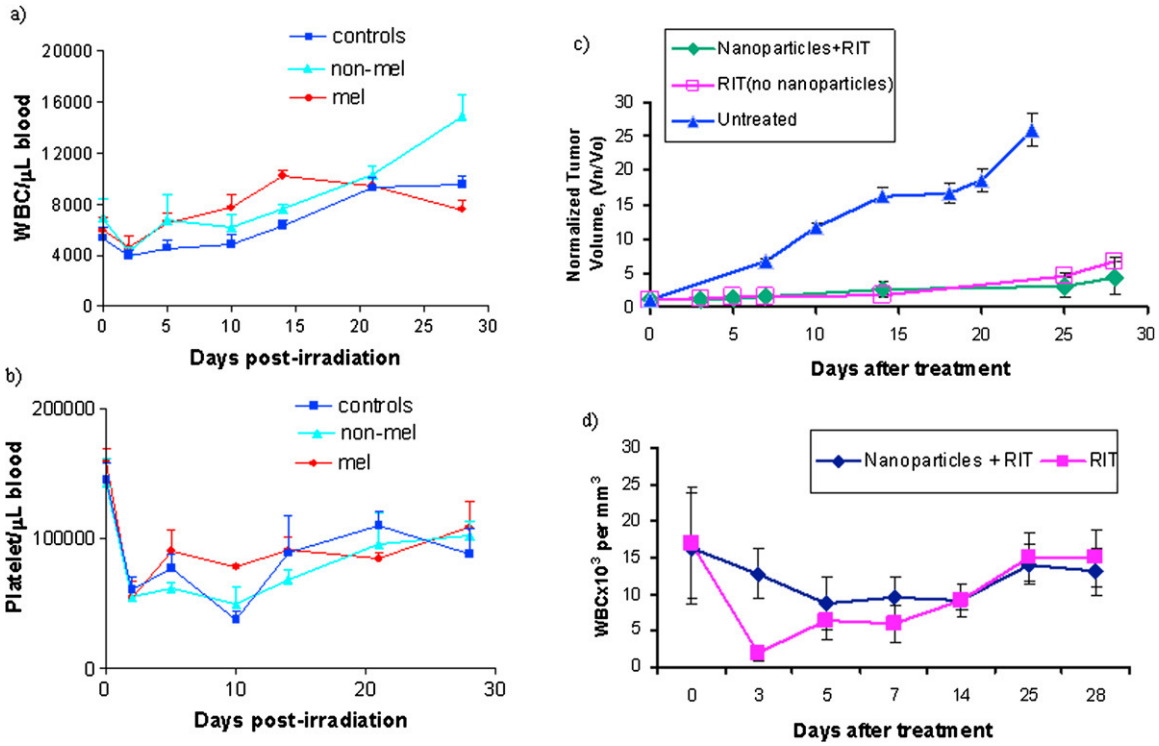


Fig. 7. Protective effects of melanin-covered nanoparticles (MNs) on the bone marrow of mice during whole-body irradiation and radioimmunotherapy (RIT). (a, b) CD-1 mice were irradiated with 125 cGy of $^{137}$Cs radiation: (a) white blood cell (WBC) counts and (b) platelet counts. controls = mice irradiated without any pre-treatment; non-mel = mice given non-melanized nanoparticles; mel = mice given MNs made with 3,4-dihydroxyphenylalanine. (c, d) Nude mice bearing A2058 melanoma tumors were given MNs 3 h before RIT with 1 mCi of $^{188}$Re-labeled 6D2 antibody to melanin. Control mice were either given RIT without MNs or left untreated. (c) Change in tumor volume after RIT treatment. (d) White blood cell counts in RIT-treated mice. The error bars represent standard error of the mean.

in the liver and spleen. These findings indicate that pretreatment or coadministration of a poloxamer would effectively increase the concentration of MNs in the bone marrow and facilitate the radioprotective objective. Poloxamers such as pluronic acid are biocompatible and have been widely used for wound healing, drug and gene delivery, and tissue engineering (28). However, in the proof-of-principle evaluation of the possible protection of bone marrow by MNs from external radiation and RIT, we chose not to administer pluronic acid to avoid any possible immunomodulatory effects of this compound, which could mask the radioprotective properties of MNs.

Measurement of WBCs and platelets in CD-1 mice receiving 125 cGy of external gamma radiation delivered at a high dose rate of 14 Gy/min showed a protective effect in mice given MNs on Days 3 to 10, which is when WBC and platelet counts nadir in irradiated mice (see relevant *P* values in the ''Results'' section). Importantly, 125 cGy is a high whole-body dose that is never given to a patient during a single session of radiation therapy because it approaches the maximum tolerated dose of 200 cGy for the bone marrow. Nevertheless, MNs afforded protection even under such conditions. The same protective effect on the bone marrow was observed in melanoma tumor–bearing mice treated with 1 mCi of RIT whereas no undesirable protection of the tumor was observed. It should be noted that because of different surface–to–body weight ratios for mice and humans, a 1-mCi dose in mice is equivalent to a 280-mCi dose in humans. Again, such high doses of radiolabeled drugs are never administered to patients in one session, which underlines the magnitude of MN protection for bone marrow. Interestingly, for both external radiation and RIT, the protection of bone marrow was observed after a single dose of MNs. Additional possibilities for improving the radioprotective properties of MNs include an increase in the administered dose, repeated dosings, and/or the use of polymers and antibodies to increase the percentage of MNs delivered to the bone marrow. We note that a silica nanoparticle may not be optimal for human therapy, given the persistence of this material in tissue. However, the method should be adaptable to biodegradable nontoxic nanospheres, given the propensity of melanin to coat many types of surfaces.

## REFERENCES

1. Hill HZ. The function of melanin or six blind people examine an elephant. *Bioessays* 1992;14:49–56.
2. Jacobson ES. Pathogenic roles for fungal melanins. *Clin Microbiol Rev* 2000;13:708–717.

3. Nosanchuk JD, Casadevall A. The contribution of melanin to microbial pathogenesis. *Cell Microbiol* 2003;5:203–223.
4. Robinson CH. Cold adaptation in Arctic and Antarctic fungi. *New Phytol* 2001;151:341–353.
5. Mironenko NV, Alekhina IA, Zhdanova NN, *et al*. Intraspecific variation in gamma-radiation resistance and genomic structure in the filamentous fungus Alternaria alternata: A case study of strains inhabiting Chernobyl reactor no. 4. *Ecotoxicol Environ Saf* 2000;45:177–187.
6. Sinilova NG, Pershina ZG, Duplitseva AP, *et al*. A radioresistant pigmented bacterial culture isolated from atomic reactor water. *Zh Mikrobiol Epidemiol Immunobiol* 1969;46:94–99.
7. Mirchink TG, Kashkina GB, Abaturov ID. Resistance of fungi with different pigments to radiation [In Russian]. *Mikrobiologiia* 1972;41:83–86.
8. Saleh YG, Mayo MS, Ahearn DG. Resistance of some common fungi to gamma irradiation. *Appl Environm Microbiol* 1988;54: 2134–2135.
9. Dadachova E, Bryan RA, Huang X, *et al*. Ionizing radiation changes the electronic properties of melanin and enhances the growth of melanized fungi. *PLoS One* 2007;5:e457.
10. Dadachova E, Bryan RA, Howell RC, *et al*. Radioprotective properties of melanin are a function of its chemical composition, free stable radical presence and spatial arrangement. *Pigment Cell Melanoma Res* 2008;21:192–199.
11. Mosse I, Kostrova L, Subbot S, *et al*. Melanin decreases clastogenic effects of ionizing radiation in human and mouse somatic cells and modifies the radioadaptive response. *Radiat Environ Biophys* 2000;39:47–52.
12. Schweitzer A, Howell RC, Jiang Z, *et al*. Physico-chemical evaluation of rationally designed melanins as novel nature-inspired radioprotectors. *PLoS One* 2009;4:e7229.
13. Pajak S, Hopwood LE, Hyde JS, *et al*. Melanin endocytosis by cultured mammalian cells. A model for melanin in a cellular environment. *Exp Cell Res* 1983;149:513–526.
14. Early PJ, Sodee DB. Principles and practice of nuclear medicine. 2nd ed. St. Louis, MO: Mosby; 1995.
15. Ito S, Fujita K. Microanalysis of eumelanin and pheomelanin in hair and melanomas by chemical degradation and liquid chromatography. *Anal Biochem* 1985;144:527–536.
16. Dadachova E, Moadel T, Schweitzer AD, *et al*. Radiolabeled melanin-binding peptides are safe and effective in treatment of human pigmented melanoma in a mouse model of disease. *Cancer Biother Radiopharm* 2006;21:117–129.
17. Dadachova E, Nosanchuk JD, Shi L, *et al*. Dead cells in melanoma tumors provide abundant antigen for targeted delivery of ionizing radiation by a monoclonal antibody to melanin. *Proc Natl Acad Sci U S A* 2004;101:14865–14870.
18. Moghimi SM. Prolonging the circulation time and modifying the body distribution of intravenously injected polystyrene nanospheres by prior intravenous administration of poloxamine-908. A 'hepatic-blockade' event or manipulation of nanosphere surface in vivo? *Biochim Biophys Acta* 1997; 1336:1–6.
19. Miale JB. Laboratory medicine hematology. St. Louis, MO: Mosby; 1982.
20. Howell RC, Revskaya E, Pazo V, *et al*. Phage display library derived peptides that bind to human tumor melanin as potential vehicles for targeted radionuclide therapy of metastatic melanoma. *Bioconjugate Chem* 2007;18:1739–1748.
21. Dadachova E, Revskaya E, Sesay MA, *et al*. Pre-clinical evaluation and efficacy studies of a melanin-binding IgM antibody labeled with (188)Re against experimental human metastatic melanoma in nude mice. *Cancer Biol Ther* 2008;7:1116–1127.
22. Pamujula S, Kishore V, Rider B, *et al*. Radioprotection in mice following oral delivery of amifostine nanoparticles. *Int J Radiat Biol* 2005;81:251–257.
23. Small W Jr.. Radiation Therapy Oncology Group C-0116 trial. Cytoprotection/radioprotection with amifostine: Potential role in cervical cancer and early findings in the Radiation Therapy Oncology Group C-0116 trial. *Semin Oncol* 2003;30(Suppl. 18):68–71.
24. Menard C, Camphausen K, Muanza T, *et al*. Clinical trial of endorectal amifostine for radioprotection in patients with prostate cancer: Rationale and early results. *Semin Oncol* 2003; 30(Suppl. 18):63–67.
25. Wakamatsu K, Ito S. Advanced chemical methods in melanin determination. *Pigment Cell Res* 2003;15:174–183.
26. Hong L, Simon JD. Current understanding of the binding sites, capacity, affinity, and biological significance of metals in melanin. *J Phys Chem B* 2007;111:7938–7947.
27. Porter CJ, Moghimi SM, Illum L, *et al*. The polyoxyethylene/polyoxypropylene block co-polymer poloxamer-407 selectively redirects intravenously injected microspheres to sinusoidal endothelial cells of rabbit bone marrow. *FEBS Lett* 1992; 305:62–66.
28. Wang Y, Liu S, Li CY, *et al*. A novel method for viral gene delivery in solid tumors. *Cancer Res* 2005;65:7541–7545.